Heat-Transfer Resistance at Solid-Liquid Interfaces: A Tool for the Detection of Single-Nucleotide Polymorphisms in DNA

15 AUTHORS, INCLUDING:

Bart van Grinsven
Maastricht University
41 PUBLICATIONS   **235** CITATIONS

SEE PROFILE

Kathia L. Jimenez- Monroy
Hasselt University
13 PUBLICATIONS   **79** CITATIONS

SEE PROFILE

Veronique Vermeeren
Hasselt University
26 PUBLICATIONS   **424** CITATIONS

SEE PROFILE

Marcel Ameloot
Hasselt University
**220** PUBLICATIONS   **3,503** CITATIONS

SEE PROFILE

Heat-Transfer Resistance at Solid−Liquid Interfaces: A Tool for the Detection of Single-Nucleotide Polymorphisms in DNA

Bart van Grinsven,[†,*] Natalie Vanden Bon,[‡] Hannelore Strauven,[†] Lars Grieten,[†] Mohammed Murib,[†] Kathia L. Jiménez Monroy,[†] Stoffel D. Janssens,[†,§] Ken Haenen,[†,§] Michael J. Schöning,[⊥] Veronique Vermeeren,[‡] Marcel Ameloot,[‡] Luc Michiels,[‡] Ronald Thoelen,[†,∥] Ward De Ceuninck,[†,§] and Patrick Wagner[†,§]

[†]Institute for Materials Research IMO, [‡]Institute for Biomedical Research BIOMED, and [§]IMEC vzw, IMOMEC, Hasselt University, Wetenschapspark 1, B-3590 Diepenbeek, Belgium, [⊥]Institute of Nano- and Biotechnologies INB, Aachen University of Applied Sciences, Heinrich-Mussmann-Strasse 1, D-52428 Jülich, Germany, and [∥]Department of Applied Engineering, XIOS University College, Agoralaan, Building H, B-3590 Diepenbeek, Belgium

The detection and identification of single-nucleotide polymorphisms (SNPs) in DNA is of central importance in genomic research for several reasons. First, SNPs are involved in hundreds of genetic disorders such as Alzheimer, mucoviscidosis, phenylketonuria, and several types of breast and colon cancer.[1,2] Second, SNPs in the so-called ADME (absorption, distribution, metabolism, excretion) genes significantly influence the effectiveness of treatment, and this is a major topic in the field of theranostics.[3] SNPs can be characterized by hybridization-based assays such as microarrays: the massive parallelized readout is an advantage, but the method requires fluorescent labeling, optical readout, and long hybridization times of ∼16 h at elevated temperatures. Furthermore, the method has an "end-point" character without providing dynamic information on molecular recognition between probe and target fragments. Finally, it is hard to unravel unknown mutations by microarrays, although there is recent progress based on refined statistical analysis allowing detecting mutated fragments in the presence of wild-type DNA.[4] Due to these drawbacks, unknown mutations are frequently identified by denaturation-based approaches. Widespread methods are real-time PCR (polymerase chain reaction) with associated melting curve analysis[5] and denaturing gradient gel electrophoresis DGGE or temperature gradient gel electrophoresis TGGE.[6,7] However, real-time PCR requires fluorescent labeling and expensive instrumentation, while DGGE is time-consuming, less suitable for parallelized analyses, and lacking information on denaturation kinetics.

ABSTRACT
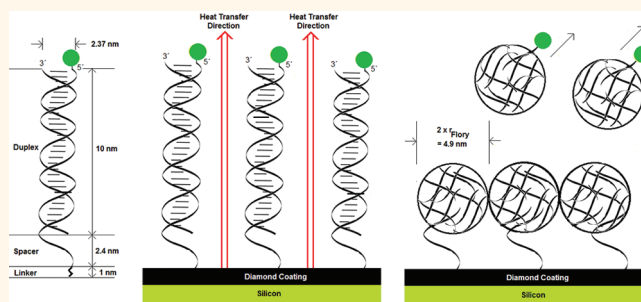
In this article, we report on the heat-transfer resistance at interfaces as a novel, denaturation-based method to detect single-nucleotide polymorphisms in DNA. We observed that a molecular brush of double-stranded DNA grafted onto synthetic diamond surfaces does not notably affect the heat-transfer resistance at the solid-to-liquid interface. In contrast to this, molecular brushes of single-stranded DNA cause, surprisingly, a substantially higher heat-transfer resistance and behave like a thermally insulating layer. This effect can be utilized to identify ds-DNA melting temperatures *via* the switching from low- to high heat-transfer resistance. The melting temperatures identified with this method for different DNA duplexes (29 base pairs without and with built-in mutations) correlate nicely with data calculated by modeling. The method is fast, label-free (without the need for fluorescent or radioactive markers), allows for repetitive measurements, and can also be extended toward array formats. Reference measurements by confocal fluorescence microscopy and impedance spectroscopy confirm that the switching of heat-transfer resistance upon denaturation is indeed related to the thermal on-chip denaturation of DNA.

To overcome these limitations, several label-free electronic and opto-electronic DNA sensor concepts have been proposed in recent literature. All of them have in common that they can operate, in principle, under hybridization and under denaturation conditions, while they can also be miniaturized and integrated in sensor arrays with a parallelized

readout. Without being exhaustive, we mention electrostatic switching effects and associated fluorescence monitoring,[8] impedance spectroscopy,[9−12] electric field-effect-based devices,[13−15] surface plasmon resonance,[16] and linear (electric) conductivity measurements through single DNA duplexes.[17] The underlying principles of these sensing effects are not yet clarified in all details, but they are presumably associated with one or several of the following phenomena, which occur upon hybridization or denaturation: change in mechanical rigidity of DNA, changes in the total charge of DNA, redistribution of counterions, and changes of the dielectric properties near the surface onto which the probe DNA is attached. Most straightforward, but especially hard to implement in a low-cost diagnostic instrument, are the conductivity measurements through single DNA molecules, which have been subject to extensive theoretical and experimental studies.[17−20] Very recently, Velizhanin et al. proposed in a theoretical study on nanoscale heat transport through individual DNA molecules that the thermal current should significantly increase upon denaturation.[21] This would offer, besides of the aforementioned (opto-) electronic approaches, an alternative access toward the detection of denaturation events and contribute to the understanding of the underlying vibrational dynamics.

In the present work, we study the temperature-dependent heat-transfer properties experimentally by using DNA brushes, in which the 5′ terminus of the probe DNA is covalently tethered to planar, temperature-controlled diamond electrodes. Although this approach is not at the single-molecule level, it offers distinct advantages: the DNA fragments are in contact with buffer medium at any time; the fragments are free to undergo conformational fluctuations; and the sensor device as such can be implemented with reasonable technological efforts. The methodology allows identifying melting temperatures by using only an adjustable heat source in combination with two temperature sensors. The sequence chosen exemplarily in this work is an exon-9 fragment of the phenylalanine hydroxylase (PAH) gene, and mutations in this gene lead to the metabolic disorder phenylketonuria.[22]

RESULTS

General Concept of the Heat-Transfer Device for DNA Chips. The principle of a heat-transfer measurement is illustrated in Figure 1A, and technical details are summarized in Methods, section titled Design of the Sensor Cell and the Thermal and Impedimetric Readout System. The central element through which the thermal current will pass is a silicon chip ($\sim$10 × 10 mm^2) covered with a thin layer of boron-doped, nanocrystalline diamond;[23] see section Preparation of the Diamond-Coated Sensor Electrodes. This diamond layer serves as an immobilization platform onto which 29-mers of

ds-DNA are covalently bound via the photochemical "fatty acid & EDC" coupling route.[24] The length of 29-mers is in line with established, commercial microarray platforms like the Affymetrix platform (25-mer oligonucleotide probes) or the Agilent system (60-mer probes); see http://corefacilities.systemsbiology.net/NucleicAcids/Microarrays/. The "fatty acid & EDC" route is applicable to various semiconductor surfaces including carbon nanowires,[25] while diamond has in addition an especially high thermal conductivity together with an outstanding chemical, electrochemical, and thermal stability. The probe ss-DNA is linked to the diamond surface via stable C−C bonds in "head-on" configuration while the target ss-DNA is free to hybridize or to denature according to experimental conditions without steric hindering (see Figure 1B,C). The sequence of the probe DNA is given in Table 1 together with the sequence of three different types of target DNA: the complement (full match), a sequence causing a CC mismatch at base pair 7, and a sequence resulting in a CC mismatch at base pair 20. The neighboring base pairs of both defects are in both cases CG and AT. The hybridization conditions (see Methods, section Functionalization of Sensor Electrodes with DNA, for details) were chosen in a way that also the defective duplexes will hybridize and be stable at room temperature. The areal density is in the order of $10^{12}-10^{13}$ duplexes per cm^2, meaning that the average distance between duplexes is less than the total length of an individual duplex.[26] For optical reference purposes, unrelated to the heat-transfer measurement itself, the target DNA fragments were carrying Alexa 488 fluorescent labels at the 5′ terminus. AFM micrographs of the chip surfaces in the subsequent stages (diamond surface, with attached fatty acid linkers, with probe DNA, and finally after hybridization with target DNA) can be found in the Supporting Information, section AFM images of NCD surfaces and the subsequent surface-functionalization steps.

This "DNA chip" was pressed mechanically with its backside onto a polished copper block, which served not only as an electrical contact but also as a heat provider (heating runs) or heat sink (cooling runs). The internal temperature of the copper block, T_1, was measured by a thermocouple and steered via a PID controller connected to a power resistor. Possible heat-transfer losses between copper and silicon were minimized by conductive silver paint. The front side of the DNA chip was exposed to 1× PBS buffer (phosphate-buffered saline solution) in a Perspex-made liquid cell: via an O-ring seal, a contact area of 28 mm^2 was defined between the chip and the liquid. Except for minor heat losses along the seal, heat will mainly be transferred from the chip to the liquid. The temperature in the liquid, T_2, was measured by a second thermocouple, positioned at a distance of 1.7 mm from the solid−liquid interface. In order to validate that a
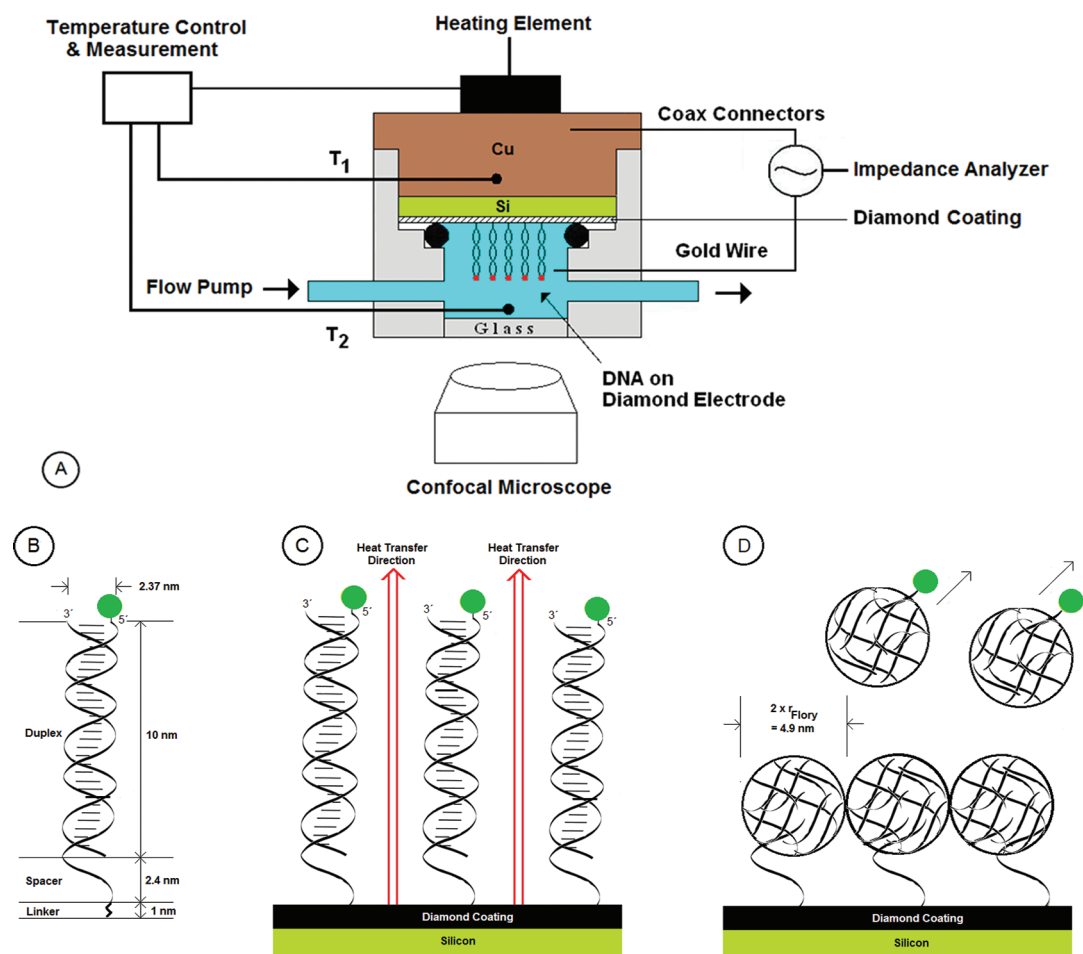
Figure 1. Top panel A shows the schematic layout of the sensor cell, allowing for the thermal monitoring of DNA denaturation together with impedimetric and optical control experiments. The probe DNA is covalently immobilized on a diamond-coated silicon electrode, while the cell is filled with PBS buffer. The temperature T_1 of the Cu backside contact is measured by a thermocouple and can be actively steered *via* a controller unit. The temperature T_2 inside the liquid is recorded by using a second thermocouple. The gold wire serves as a counter electrode for impedance measurements, and the glass window provides optical access. The heat-transfer related parameters are the temperature difference $T_1 - T_2$ and the input power P provided by the heating element. Panel B sketches the DNA duplexes with labeled target strands, and panel C illustrates the heat-transfer path through a molecular DNA brush. After denaturation, the probe DNA curls up in irregular structures characterized by the Flory radius, thus hindering the solid-to-liquid heat transfer (panel D).

TABLE 1. Compilation of the Base Sequences of the Probe DNA and the Three Different Types of Target DNA Employed in the Hybridization and Denaturation Experiments[a]

	sequence	T_m (°C)
ss-DNA (probe)	3′-CCA AGC CCC CAT ATG TAC CCG ACG TCC CC - A AAA AAA C$_6$H$_{12}$-NH$_2$-5′	
ss-DNA full match	5′-Alexa-C$_6$H$_{12}$ GGT TCG GGG GTA TAC ATG GGC TGC AGG GG-3′	79.5
ss-DNA 1MM BP7	5′-Alexa-C$_6$H$_{12}$ GGT TCG GGG GTA TAC ATG GGC T**C**C AGG GG-3′	76.7
ss-DNA 1MM BP20	5′-Alexa-C$_6$H$_{12}$ GGT TCG GGG **C**TA TAC ATG GGC TGC AGG GG-3′	75.0

[a] The probe DNA exhibits a spacer consisting of seven A bases, while the target DNA fragments carry a fluorescent Alexa 488 label at the 5′ end. The position of the mismatches with respect to the probe DNA is underlined and indicated by bold letters. The third column lists the calculated melting temperatures based on the HyTher algorithm, reflecting the relative stability of the complementary and the mismatched DNA duplexes.

heat-transfer measurement can indeed give information on DNA binding or denaturation, the cell also featured a gold electrode in the liquid, which was connected, together with the copper backside contact, to a homemade impedance analyzer.[27] Furthermore, a glass window allowed for optical monitoring with an inverted confocal fluorescence microscope (see

Methods, section Confocal Fluorescence Microscopy). Unless stated otherwise, the heat-transfer device was operated in a temperature-stabilized environment at 19.3 ± 0.1 °C.

Heat Transfer Measurements with Fluorimetric and Impedimetric Control. The first series of measurements, described in this section, refers to the most stable, fully

complementary duplexes in combination with a diamond-coated silicon electrode denoted as #D1. During the measurement, T_1 was increased with a heating rate of 1 °C/min from 35 to 90 °C and cooled back to 35 °C at the same rate by reducing the heating power. This was performed for three consecutive heating/cooling runs, and the time dependence of T_1 and T_2 is shown in Figure 2. Note that, during the first heating, an anomalous behavior of T_2 occurs, highlighted with a circle, which was absent during the second and the third run. This first-run temperature anomaly was also found with three other electrodes (#D2, #D3, and #D4), meaning that the effect appears to be intrinsic and most probably related to thermally induced DNA denaturation. In order to prove this assumption, the first and second heating run experiment was repeated with simultaneously measuring also the impedance of the sensor cell and monitoring the fluorescence intensity on the electrode surface. These measurements were performed at nonregulated room temperature (about 22 °C), and we verified that there was no measurable heat input by the laser beam into the system.

Figure 3 summarizes the data obtained with three independent methods, confirming the assumption that DNA denaturation has indeed an impact on the heat-transfer properties of the device. The temperature (T_1) dependence of the fluorescence intensity signal from the electrode surface is shown in Figure 3A: denaturation sets in at 47 °C and terminates at 55 °C, where the fluorescence intensity drops to its background value, which originates from strayed laser light. The denatured sample shows this background intensity at all temperatures. The midpoint temperature of the fluorescence intensity decay is found at 49.7 ± 0.3 °C. Labeled target DNA, removed from the immobilized probe DNA during denaturation, cannot contribute to the signal anymore because the confocal volume is limited to a maximum of 5 μm above the chip surface, which is negligible as compared to the total cell volume. This fluorescence test is a stringent and independent control because it is electronically and physically decoupled from the rest of the setup, which is steering and monitoring T_1 and T_2 and measuring the impedance values. Therefore, the fluorescence data are definitely free of any hypothetical crosstalk effects. Confocal images of the denaturation process are included in the Supporting Information, section Confocal fluorescence images during thermal DNA denaturation. Figure 3B shows the T_1 dependence of the amplitude and the phase angle of the impedance signal at a frequency of 1058 Hz, avoiding possible noise input from the 50 Hz power grid. Below 47 °C, the double- and the single-stranded DNA electrode behave differently in impedance amplitude and in phase angle while they coincide for temperatures above 57 °C. The impedance amplitude of the first heating run (denaturation) clearly shows a local
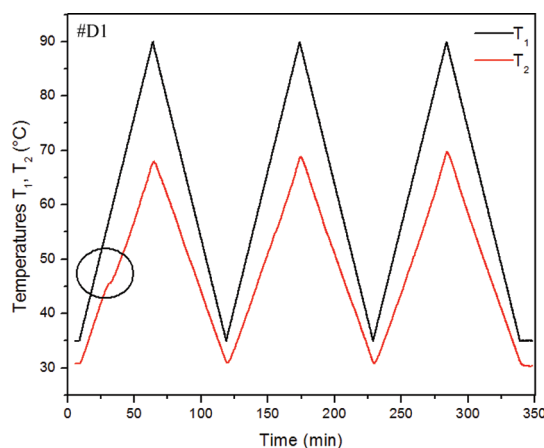

Figure 2. Three subsequent heating and cooling cycles performed with electrode #D1 with immobilized probe DNA. As a starting condition, the probe DNA was hybridized with the complementary target, and the anomalous behavior of the liquid temperature T_2 (indicated with a circle) during the first heating run is associated with the double-helix melting. The black solid line is the temperature T_1 of the Cu backside contact, and the liquid temperature T_2 is shown as a red solid line. For heating and cooling, the temperature T_1 is increased or reduced at a rate of 1 °C/min.

maximum at 49.5 ± 0.2 °C, which corresponds nicely to the midpoint temperature of the fluorescence decay curve. We mention that the impedance results are a superposition of two effects: the surface impedance of electrodes with ds- *versus* ss-DNA is different as reported earlier,[12] but also, the impedance of the buffer solution depends sensitively on temperature. More details are given in the Supporting Information, section Discussion of the impedance signal upon crossing the DNA-melting transition.

The top-right of Figure 3C shows the temperature difference $\Delta T = T_1 - T_2$ as a function of T_1, with the black curve corresponding again to the first heating run while the red curve presents the second heating with only ss-DNA on the chip. Both curves coincide at temperatures above 55 °C, where the melting transition is completed. Figure 3C also includes the temperature dependence of the electrical heating power P (T_1), which was required to achieve the linear increase of T_1 according to the heating rate of 1 °C/min. Also here, there is a difference between the ds- and ss-DNA chip, which disappears above 55 °C. In order to extract the heat-transfer resistance R_{th} quantitatively, we analyzed for all temperatures T_1 the ratio of the temperature difference $\Delta T = T_1 - T_2$ and the input power P according to $R_{th} = \Delta T/P$ (see, for example, ref 28). The resulting data are summarized in Figure 3D. The somewhat noisy appearance is related to the fact that we show nonfiltered, raw data obtained in an environment without active temperature control: while the temperature T_1 is strictly linear and smooth in time, the required heating power shows small fluctuations within short time periods. In case of the ds-DNA chip, we find a low-temperature value of $R_{th} = 7.7$ °C/W, which
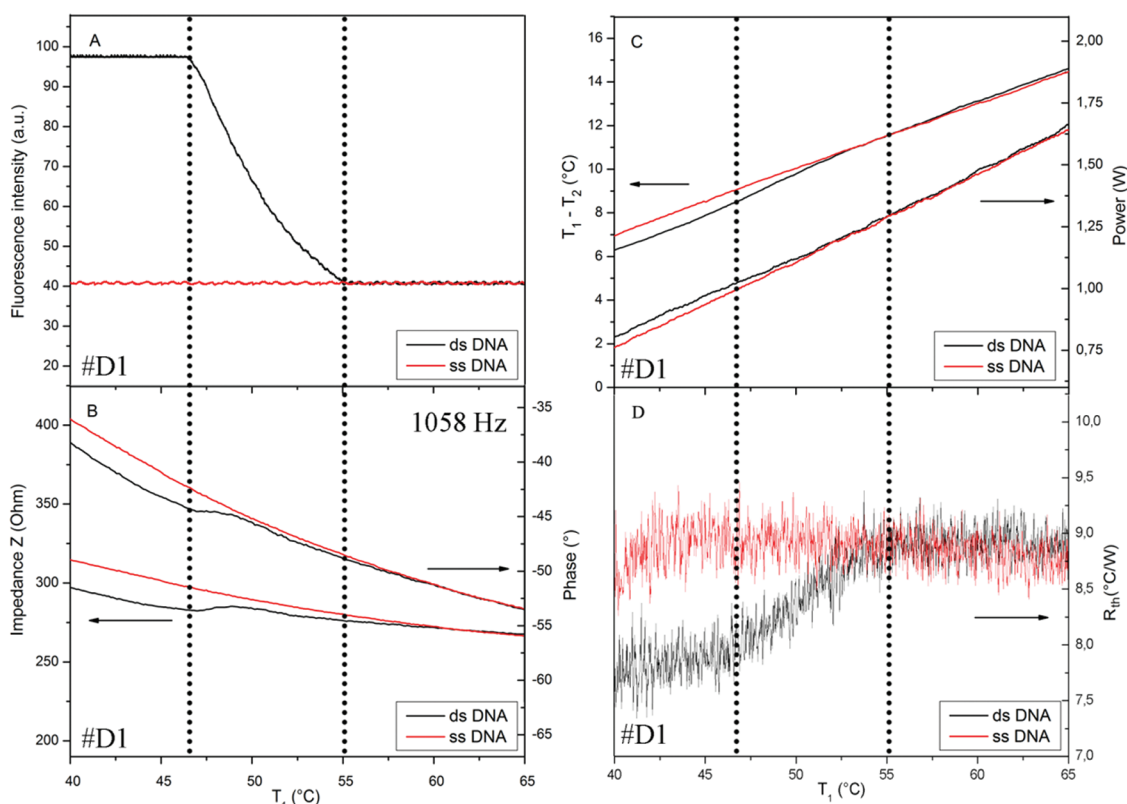
Figure 3. Compilation of simultaneously measured fluorescence-intensity data (A) impedance data (B) and heat-transfer related data (C,D) obtained for electrode #D1 with complementary ds-DNA (first heating run in black solid lines) and subsequently with ss-DNA (second heating run, red solid lines). Fluorescence indicates that denaturation starts at 47 °C and is completed at 55 °C. This is also the temperature range where the amplitude and phase of the impedance signals (here at 1058 Hz) converge. Panel C shows the temperature difference $\Delta T = T_1 - T_2$ as a function of T_1 (temperature of the copper back contact) together with the T_1 dependence of the heating power P at the right-hand axis. The heat-transfer resistance R_{th}, being the ratio $\Delta T/P$, is given in panel D. All data are raw data without further processing.

starts to increase around 46 °C and reaches a new equilibrium value of 8.9 °C/W at and above 55 °C (black curve). The midpoint of the transition is found at $T_{\text{midpoint}} = 49.2 \pm 0.5$ °C, which is again close to the midpoint temperature of the fluorescence decay curve. Performing the same R_{th} analysis with the ss-DNA chip during the second heating run resulted in an almost temperature-independent R_{th} of 8.9 °C/W (red curve). This increase of the absolute R_{th} value by ∼1.2 °C/W (16% increase) upon denaturation is a substantial effect, keeping in mind that the DNA brush is only a miniscule component (the fragment length corresponds to 10 nm) as compared to the total heat-transfer path with a distance of almost 3 mm between the two thermocouples. The effect size is also more than twice as strong as the denaturation-induced change of the impedance amplitude with an increase by about 7%. From these observations, we conclude that the temperature anomaly documented in Figure 2 (first heating run) is one-to-one related to the thermally induced denaturation of ds-DNA, which changes the heat transfer resistance at the solid−liquid interface.

Studies on Various Chip Surfaces and DNA with Sequence Defects. In the following, we will describe experiments performed with the diamond electrode #D2 in a

temperature-stabilized environment (see Figure 4). First, the as-grown diamond chip was oxidized with a UV-ozone treatment to obtain a hydrophilic surface termination, which is stable in aqueous solutions. The R_{th} value is about 6.7−7.0 °C/W and widely temperature-independent (red line). Attaching the fatty acid cross-linker molecules (purple line) also resulted in a temperature-independent R_{th}, which cannot, within the experimental resolution, be distinguished from the behavior of the oxygen-terminated surface. In principle, this does not come as a surprise because the dense molecular brush of alkyl chains consisting of 10 carbon atoms is not longer than 1 nm. Attaching the single-stranded probe DNA made the R_{th} rise to 9.0 °C/W at 40 °C with a monotonous decrease to 8.4 °C/W at 80 °C. This sample was subsequently hybridized with complementary target DNA (black line), target DNA with a CC mismatch at base pair 7 (green line), and target DNA with the CC mismatch at base pair 20 (orange line). Note that the three hybridizations were performed with the original probe DNA on the sensor chip without any kind of surface regeneration. All curves exhibit the stepwise increase of R_{th} upon denaturation with midpoint temperatures of 63.0 ± 0.1 °C for the complement, 57.6 ± 0.1 °C for the mismatch at
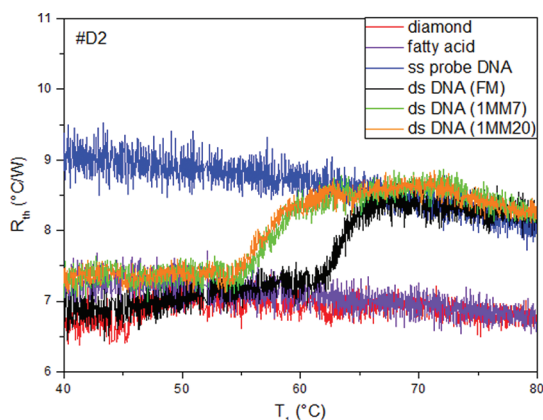
Figure 4. Heat-transfer resistance R_{th} as a function of temperature for electrode #D2 (data have not been filtered): the unmodified electrode (red line) and the electrode with covalently attached fatty acid linkers (purple line) have a widely temperature-independent R_{th} around 7 °C/W. In the configuration with attached probe DNA (blue line), the heat-transfer resistance has notably increased to 9 °C/W, indicating an efficient thermal insulation by the highly flexible ss-DNA fragments. The R_{th} of double-stranded DNA (black line for the complementary duplexes) is comparable to the nonmodified surface at low temperatures and switches to the ss-DNA behavior upon denaturation with a midpoint temperature $T_{midpoint} = 63.0 \pm 0.1$ °C. Repeating the experiment with defective DNA duplexes results in a clear shift of $T_{midpoint}$ to lower temperatures: for the duplex with CC mismatch at BP 7 (green line), we obtain $T_{midpoint} = 57.6 \pm 0.1$ °C, and for the same mismatch at BP 20 (orange line), this is 56.8 ± 0.1 °C. The relative order of stability corresponds to the calculated data given in Table 1.

base pair 7, and 56.8 ± 0.1 °C for the mismatch at base pair 20. The relative order of stability agrees nicely with calculated melting temperature values summarized within Table 1. These calculations were based on the online HyTher algorithm (http://ozone3.chem.wayne.edu/), taking into account the lengths of fragments, the identity and orientation of neighboring bases, the ionic strength of the buffer, and the fact that all fragments are tethered at one end. We point out that our denaturation temperatures are lower than the predicted values; however, the fluorescence control renders the experimental data unquestionable. Moreover, the same order of stability was confirmed with the three other DNA chips (#D1, #D3, and #D4).

Finally, Table 2 summarizes all $T_{midpoint}$ and R_{th} data for the four different DNA chips under study regarding the thermal denaturation of the most stable, complementary DNA duplexes. All data were obtained from measurements in the temperature-stabilized environment of 19.3 °C. In the case of #D3, the measurement was performed in three-fold (run a, run b, and run c) with a complete regeneration of the sensor surface between run b and run c, meaning that the fatty acid and probe DNA layers were etched off in oxygen plasma and built up for a second time. There is a certain sample-to-sample variation of the midpoint temperatures, and we attribute this to the manual mounting of the DNA chip in the sensor device,

possibly in combination with minor fluctuations in the precise size of the chips and the thickness and grain size of their diamond coatings. When looking at the intrasample variability, it can be seen that the subsequent runs a and b performed with sample #D3 deliver practically identical results, and only after the complete surface regeneration, a certain shift of $T_{midpoint}$ occurs. Despite this, the absolute change of R_{th} upon denaturation is remarkably constant and has for all DNA chips a value between 1.3 and 1.5 °C/W. To determine the jump height, ΔR_{th}, we calculated the difference between R_{th} measured at 10 °C above $T_{midpoint}$ and the corresponding value 10 °C below $T_{midpoint}$, in both cases clearly outside the regime of the melting transition. The universal amplitude of ΔR_{th} strongly supports the idea of a universal feature, which is independent of the employed sensor chip. Data obtained with heating rates of 0.5 and 2.0 °C/min are shown in the Supporting Information, section Heat-transfer resistance measured with different heating rates.

DISCUSSION

The increase of R_{th} upon denaturation has to our knowledge not been reported in prior literature, and there is also no explanation yet based on first-principles calculations. The theoretical work of Velizhanin *et al.* predicts actually an enhanced heat transfer by single-stranded DNA, but the boundary conditions are different (DNA molecule under dry conditions, clamped between two heat reservoirs with a fixed temperature difference) and modeling parameters come into play.[21] The experimental thermal and electronic conductivity studies by Kodama *et al.* on individual ds-DNA fragments combined with gold nanoparticles are also not comparable to our approach: These measurements under vacuum conditions (temperature regime 100−300 K) did not cross the melting transition, and both fragment ends were tethered to gold contacts, limiting the mechanical freedom of the molecules.[29]

However, we can clearly state that the observed impact of denaturation on the heat-transfer resistance cannot be explained by a calorimetric effect. Calorimeters measure interaction energies during a molecular recognition or unbinding process and have been employed in classical DNA studies[30,31] and, more recently, in the context of synthetic receptors.[32,33] Here, we find a persistent change of R_{th} from low values at all temperatures below the melting transition to higher values at all temperatures above this transition, an effect which is not restricted to the melting transition itself. The fact that ds-DNA does not measurably increase the heat-transfer resistance can be understood on the following grounds: the fragments of 29 base pairs have a length of 10 nm, which is far below the estimated persistence

TABLE 2. Compilation of the *T* Midpoint and Heat-Transfer Data of Thermally Induced Denaturation of Complementary DNA Duplexes Obtained with Four Different Diamond Electrodes[a]

	#D1	#D2	#D3 (run a)	#D3 (run b)	#D3 (run c)	#D4
$T_{midpoint}$ (°C)	52.5 ± 0.2	63.0 ± 0.1	53.5 ± 0.2	53.5 ± 0.1	56.5 ± 0.1	52.0 ± 0.3
R_{th} (°C/W) ss state	8.9 ± 0.2	8.6 ± 0.1	8.6 ± 0.1	8.7 ± 0.2	8.7 ± 0.1	8.7 ± 0.3
R_{th} (°C/W) ds state	7.6 ± 0.2	7.1 ± 0.2	7.3 ± 0.2	7.3 ± 0.2	7.4 ± 0.2	7.2 ± 0.2
ΔR_{th} (°C/W)	1.3 ± 0.2	1.5 ± 0.1	1.3 ± 0.2	1.4 ± 0.2	1.3 ± 0.2	1.5 ± 0.2

[a] The data with electrode #D3 were measured in three-fold (runs a, b, and c) with a complete sensor regeneration between run b and run c. The R_{th} values of the single-stranded state were measured at 10 °C above $T_{midpoint}$, while the corresponding R_{th} in the double-stranded state was taken at 10 °C below $T_{midpoint}$. Note that the jump height ΔR_{th} is remarkably constant and independent of the electrode or the midpoint temperature, suggesting an intrinsic effect of the DNA brush on the total heat-transfer resistance of the device.

length of 50 nm.[34,35] Therefore, these fragments can be considered as "stiff rods" on the chip surface with a tilt angle in the range of 31−52°.[36,37] Most publications agree that the areal density of ds-DNA is, irrespective of the immobilization method, in the range from 10^{12} to 10^{13} duplexes per cm²; see ref 26 and references therein. The most probable areal density in our case, as determined by X-ray photoemission spectroscopy, is 8×10^{12}/cm² [H. Yin and H.-G. Boyen, manuscript in preparation]. With a diameter of 2.37 nm for ds-DNA, we conclude that about 35% of the chip surface is dressed with ds-DNA, while the remaining surface fraction of 65% still represents the unaltered solid−liquid interface (see Figure 1C for a schematic illustration). The unaltered surface transfers thermal energy from the phonons in the diamond lattice to the water molecules, while there is also recent evidence that the heat transfer along ds-DNA is based on molecular vibrations.[29] After denaturation, we are dealing with fragments with a total length of 36 nucleotides (L = 12.24 nm), while the persistence length drops to l_p = 1.48 nm.[34] Therefore, the ss-DNA curls up in irregular shapes, and the typical Flory radius can be approximated according to $r_{Flory} = (l_p \times L/3)^{1/2}$.[35] This results in r_{Flory} = 2.46 nm. On the basis of the presence of 8×10^{12} ss-DNA fragments per cm², the surface coverage increases to nominally 150%, corresponding to a densely covered surface. Therefore, we suppose that denaturation brings about major parts of the sample surface being covered with random coils of ss-DNA, which interrupts the heat-transfer channel from the phonons in the solid to the liquid. A visualization of the situation in the denatured state is given in Figure 1D. From $\Delta R_{th} \sim$ 1.5 °C/W, the size of the solid−liquid interface (28 mm²), and an areal density of 8×10^{12}/cm² ss-DNA fragments, we conclude that each curled-up fragment can be considered as an individual thermal resistor R_{th}^{*}(ss-DNA) with a value of about 3.4×10^{12} °C/W. Interestingly enough, Velizhanin *et al.* predict for individual ds-DNA fragments a thermal conductivity of $\sigma_{th} = 1.8 \times 10^{-2}$ W/(°C·m) at 300 K.[21] Considering the 29-mer fragments as stiff rods with a length of 10 nm and a nominal radius of 1.2 nm, this conductivity translates to a resistance R_{th}^{*}(ds-DNA) = 1.2×10^{12} °C/W or roughly one-third of the value we derived experimentally for the disordered, single-stranded

state. Despite of the good agreement well within the same order of magnitude, this comparison is not yet stringent because in our case a substantial part of the thermal current in the ds-DNA state passes through the 65% surface fraction where the sensor surface is in direct contact with the buffer solution.

Besides the considerations on the underlying principle of the heat-transfer effect, the method should, of course, be applicable in genetic research, where high-throughput analysis and parallelization are important aspects. The fact that DNA on diamond electrodes can be denatured and rehybridized for at least 30 times without loss of binding capacity is already highly beneficial for serial analyses.[38] Moreover, the current hybridization time of 120 min (see Methods, section Functionalization of Sensor Electrodes with DNA) can be shortened by employing higher concentrations of target fragments, by increasing the temperature to facilitate diffusion, or by a higher ionic strength of the hybridization buffer. This way, hybridization times in the order of 20 min are reported in literature.[14] Whether an accelerated hybridization would have an adverse influence on the precision of the heat-transfer technique is not yet clarified; however, there is evidence that the current protocol guarantees a one-to-one correspondence between the numbers of probe DNA and target DNA fragments.[26] Comparing the 8×10^{12} fragments per cm² to the cell volume of 110 μL results in a concentration of target molecules of 34 nM, corresponding in turn to $\Delta R_{th} \sim$ 1.5 °C/W. Smoothening of the R_{th} data will easily allow one to identify R_{th} changes on the order of 0.1 °C/W, meaning that the detection limit is about 2 nM. For comparison, the detection limit obtained for oligonucleotides with label-free surface plasmon imaging is 10 nM,[39] and micromechanical sensors operate with target DNA concentrations of 100 nM or higher.[40]

The first step toward an array format would be the miniaturization of the sensing electrodes, and diamond-based electrodes on glass substrates with a diameter below 100 μm have been documented in the literature.[41] Also, diamond nanowires with a thickness even below 10 nm have been fabricated by reactive ion etching.[42] The functionalization of these micro- and nanostructures with selected probe and

target DNA can, for example, be achieved by dip-pen nanolithography.[43] A bigger challenge would be the development of an array-type detection system, more specifically, an array of planar thermocouples with a contact area comparable to the size of the sensor spots. Here, the present state-of-the-art systems are thermocouple arrays with an area of a few square micrometers of each junction,[44] which looks most feasible to detect the heat flow through the individual sensor spots with sufficient spatial resolution to minimize crosstalk between neighboring spots.

In conclusion, we propose that label-free heat-transfer monitoring should be considered as a promising, inexpensive, and real-time alternative to the currently used denaturation-based techniques for DNA characterization and the identification of new point mutations. Moreover, the heat-transfer effect is certainly not limited to diamond surfaces alone, and it may also be useful in monitoring other biomolecular interactions on solid supports. Finally, the method may serve as a characterization technique for the areal density and conformational aspects of molecular polymer brushes in general.

METHODS

Design of the Sensor Cell and the Thermal and Impedimetric Readout System. The sensor setup shown in Figure 1 was described earlier in the context of chemical denaturation studies.[12] The flow cell has an inner volume of 110 μL, and liquids can be exchanged with a syringe-driven flow system (ProSense, model NE-500, The Netherlands). All measurements described here were performed under static conditions. For heat-transfer measurements, the device was now equipped with two miniaturized thermocouples (type K, diameter 500 μm, TC Direct, The Netherlands) monitoring the temperature T_1 of the copper backside contact and the liquid temperature T_2 at a position in the center of the flow cell at 1.7 mm above the chip surface. The heat flow was generated with a power resistor (22 Ω, MPH 20, Farnell, Belgium) glued onto the copper block with heat-conductive paste and tightly fixed with a screw. To regulate T_1, the thermocouple signal was led to a data acquisition unit (Picolog TC08, Picotech, United Kingdom) and from there processed into a PID controller (parameters: $P = 10$, $D = 5$, $I = 0.1$). The calculated output voltage was sent via a second controller (NI USB 9263, National Instruments, USA) to a power operational amplifier (LM675, Farnell, Belgium) and fed into the power resistor. Sampling of the T_1 and T_2 values was done at a rate of one measurement per second. For impedance monitoring, the counter electrode was a gold wire (500 μm diameter), also at a distance of 1.7 mm from the surface of the diamond working electrode, but spanning the entire diameter of the liquid cell (5 mm). There was no measurable electronic crosstalk between the impedance spectroscopy and the temperature regulation unit. The impedance unit (see ref 27 for circuitry details) measured the impedance in the frequency range of 100 Hz to 100 kHz with 10 frequencies per decade on a logarithmic scale and a scanning speed of 5.7 s per sweep. All data presented here refer to a frequency of 1058 Hz, ensuring an optimal signal-to-noise ratio. The amplitude of the ac voltage, applied under open circuit conditions, was fixed to 10 mV$_{rms}$.

Preparation of the Diamond-Coated Sensor Electrodes. The nanocrystalline diamond-coated sensor electrodes were prepared by plasma-enhanced chemical vapor deposition from methane/hydrogen mixtures (3% CH$_4$) in an ASTeX reactor.[23] The substrates were 2 in. silicon wafers (thickness 500−550 μm, crystalline orientation (100), p-type doped with resistivities from 1 to 20 $\Omega \cdot$cm), which were diced into chips after deposition. The diamond layers had a thickness of 100 nm and an average grain size of 50 nm. To ensure a good electrical conductivity of the coating ($\sim$1 $\Omega \cdot$cm), the deposition was done with an admixture of trimethyl borane gas to the CH$_4$ with a ratio of 200 ppm B/C. The as-prepared electrodes were hydrogenated in H$_2$ plasma (50 Torr, 800 °C, power 4000 W for 14 min) to obtain hydrophobic surfaces prior to the photochemical attachment of the fatty acid linker molecules. Here, we employed 10-undecanoic fatty acid (purchased from Sigma-Aldrich), which was tethered with its hydrophobic C=C terminus to the electrodes by UV illumination (wavelength 254 nm, intensity 265 mW/cm^2) for 20 h under N$_2$ atmosphere. A reaction mechanism for this covalent binding process was recently proposed by Wang et al.[45] After

this photochemical step, the samples were rinsed in acetic acid at 100 °C to release unbound fatty acid fragments.

Functionalization of Sensor Electrodes with DNA. The probe ss-DNA (purchased from Invitrogen) was a 36-mer (see Table 1) with a NH$_2$-modified 5′ terminus allowing for a covalent linking to the COOH group of the fatty acid by using carbodiimide (EDC) coupling. EDC was purchased from Perbio Science, and details of this procedure are published in ref 26. The first seven adenine bases at the 5′ terminus served as a spacer to minimize steric hindering during hybridization due to the proximity of the solid surface. The total amount of probe ss-DNA used to functionalize 1 cm^2 of electrode surface was 300 pmol. This actually exceeds the binding capacity of the surface but ensures a rapid functionalization. Nonreacted probe DNA was rinsed off by washing the samples for 30 min in homemade 2× SSC buffer (sodium chloride/sodium citrate) with 0.5% SDS (sodium dodecyl sulfate) at room temperature. Hybridization with the 29-mer target DNA (from Invitrogen) was performed by incubating these samples for 2 h at 30 °C with 600 pmol of target fragments in 10× PCR buffer (homemade). During hybridization, the samples were kept under a saturated water vapor atmosphere to avoid evaporation of the reaction fluid. After hybridization, nonreacted target DNA was removed by rinsing again with 2× SSC buffer with 0.5% SDS (30 min, room temperature), followed by two 5 min rinsing steps, once in 2× SSC buffer and once in 0.2× SSC buffer, both at room temperature. Reference tests with a hybridization temperature of 50 °C confirmed that the temperature of the melting transition is insensitive to the hybridization temperature.

Confocal Fluorescence Microscopy. For fluorescence intensity studies and photobleaching experiments, a Zeiss LSM 510 META Axiovert 200 M laser scanning confocal fluorescence microscope was used. Excitation of the Alexa Fluor 488 labels was done with the 488 nm emission line of an argon ion laser with a maximum intensity at the sample surface of 1.00 ± 0.05 mW. The settings of the filters and the confocal optics are documented in ref 26; the confocal volume had a diameter of 0.44 μm and a height of 5 μm. All images were collected with a 10×/0.3 Plan Neofluar air objective with a working distance of 5.6 mm. The image size was 128 × 128 with a pixel dwell time of 51.2 μs, corresponding to a total scanned area of $\sim$225 × 225 μm^2. The pinhole size was 150 μm, and the laser intensity was set at 10%, corresponding to a power input of 33 μW on the chip surface. The detector gain, a measure for the photomultiplier voltage, was set at 1000 for all measurements. After hybridization with the different types of labeled target DNA, the fluorescence of each DNA chip was studied to ensure the presence and homogeneous distribution of DNA. Moreover, bleaching experiments (laser intensity set to 100% for 15 min, bleached area of 20 × 200 μm^2) confirmed that the fluorescence intensity originated from the Alexa 488 dyes and not from the underlying diamond layer. The bleached areas served also to define the remnant background intensity due to strayed or reflected laser light. The fluorescence intensity decay during denaturation was monitored at a frequency of one confocal image taken every 1.4 s, and the area-averaged intensities were retrieved using the

ImageJ1.44 software package. All intensities measured after denaturation were in full agreement with the remnant intensities found before on bleached regions, meaning that the data are not affected by laser-intensity fluctuations.

Conflict of Interest: The authors declare no competing financial interest.

Supporting Information Available: Additional figures and discussion. This material is available free of charge *via* the Internet at http://pubs.acs.org.

REFERENCES AND NOTES

1. Schon, E. A.; Bonilla, E.; DiMauro, S. Mitochondrial DNA Mutations and Pathogenesis. *J. Bioenerg. Biomembr.* **1997**, *29*, 131–149.

2. Dunning, A. M.; Healey, C. S.; Pharoah, P. D. P.; Teare, M. D.; Ponder, B. A. J.; Easton, D. F. A Systematic Review of Genetic Polymorphisms and Breast Cancer Risk. *Cancer Epidemiol., Biomarkers Prev.* **1999**, *8*, 843–854.

3. Hooper, J. W. The Genetic Map to Theranostics. *MLO* **2006**, *38*, 22–35.

4. Hooyberghs, J.; Carlon, E. Hybridisation Thermodynamic Parameters Allow Accurate Detection of Point Mutations with DNA Microarrays. *Biosens. Bioelectron.* **2010**, *26*, 1692–1695.

5. Tindall, E. A.; Petersen, D. C.; Woodbridge, P.; Schipany, K.; Hayes, V. M. Assessing High-Resolution Melt Curve Analysis for Accurate Detection of Gene Variants in Complex DNA Fragments. *Human Mutat.* **2009**, *30*, 876–883.

6. Fodde, R.; Losekoot, M. Mutation Detection by Denaturating Gradient Electrophoresis. (DGGE). *Human Mutat.* **1994**, *3*, 83–94.

7. Muyzer, G.; Smalla, K. Application of Denaturing Gradient Gel Electrophoresis (DGGE) and Temperature Gradient Gel Electrophoresis (TGGE) in Microbial Ecology. *Antonie van Leeuwenhoek* **1998**, *3*, 127–141.

8. Rant, U.; Arinaga, K.; Sherer, S.; Pringsheim, E.; Fujita, S.; Yokoyama, N.; Tornow, M.; Abstreiter, G. Switchable DNA Interfaces for the Highly Sensitive Detection of Label-Free DNA Targets. *Proc. Natl. Acad. Sci. U.S.A.* **2007**, *104*, 17364–17369.

9. Katz, E.; Willner, I. Probing Biomolecular Interactions at Conductive and Semiconductive Surfaces by Impedance Spectroscopy: Routes to Impedimetric Immunosensors, DNA-Sensors and Enzyme Biosensors. *Electroanalysis* **2003**, *15*, 913–947.

10. Vermeeren, V.; Bijnens, N.; Wenmackers, S.; Daenen, M.; Haenen, K.; Williams, O. A.; Ameloot, M.; vandeVen, M.; Wagner, P.; Michiels, L. Towards a Real-Time, Label-Free Diamond-Based DNA Sensor. *Langmuir* **2007**, *23*, 13193–13202.

11. Park, J. Y.; Park, S. M. DNA Hybridization Sensors Based on Electrochemical Impedance Spectroscopy as a Detection Tool. *Sensors* **2009**, *9*, 9513–9532.

12. van Grinsven, B.; Vanden Bon, N.; Grieten, L.; Murib, M.; Janssens, S. D.; Haenen, K.; Schneider, E.; Ingebrandt, S.; Schöning, M. J.; Vermeeren, V.; *et al*. Rapid Assessment of the Stability of DNA Duplexes by Impedimetric Real-Time Monitoring of Chemically Induced Denaturation. *Lab Chip* **2011**, *11*, 1656–1663.

13. Poghossian, A.; Cherstvy, A.; Ingebrandt, S.; Offenhäusser, A.; Schöning, M. J. Possibilities and Limitations of Label-Free Detection of DNA Hybridization with Field-Effect-Based Devices. *Sens. Actuators, B.* **2005**, *111*, 470–480.

14. Ingebrandt, S.; Han, Y.; Nakamura, F.; Poghossian, A.; Schöning, M. J.; Offenhäusser, A. Label-Free Detection of Single Nucleotide Polymorphisms Utilizing the Differential Transfer Function of Field-Effect Transistors. *Biosens. Bioelectron.* **2007**, *22*, 2834–2840.

15. Kawarada, H.; Ruslinda, A. R. Diamond Electrolyte Solution Gate FETs for DNA and Protein Sensors Using DNA/RNA Aptamers. *Phys. Status Solidi A* **2011**, *208*, 2005–2016.

16. Kick, A.; Boensch, M.; Katschner, B.; Voight, J.; Herr, A.; Brabetz, W.; Jung, M.; Sonntag, F.; Klotzbach, U.; Danz, S.; *et al*. DNA Microarrays for Hybridization Detection by Surface Plasmon Resonance Spectroscopy. *Biosens. Bioelectron.* **2010**, *26*, 1543–1547.

17. Guo, X. F.; Gorodetsky, A. A.; Hone, J.; Barton, J. K.; Nuckolls, C. Conductivity of a Single DNA Duplex Bridging a Carbon Nanotube Gap. *Nat. Nanotechnol.* **2008**, *3*, 163–167.

18. Dekker, C.; Ratner, M. Electronic Properties of DNA. *Phys. World* **2001**, *14*, 29–33.

19. Cuniberti, G.; Craco, L.; Porath, D.; Dekker, C. Backbone-Induced Semiconducting Behavior in Short DNA Wires. *Phys. Rev. B* **2002**, *65*, 241314.

20. Cohen, H.; Nogues, C.; Naaman, R.; Porath, D. Direct Measurement of Electrical Transport through Single DNA Molecules of Complex Sequence. *Proc. Natl. Acad. Sci. U.S.A.* **2005**, *102*, 11589–11593.

21. Velizhanin, K. A.; Chien, C. C.; Dubi, Y.; Zwolak, M. Driving Denaturation: Nanoscale Thermal Transport as a Probe of DNA Melting. *Phys. Rev. E* **2011**, *83*, 050906.

22. Guldberg, P.; Rey, F.; Zschocke, J.; Romano, V.; Francois, B.; Michiels, L.; Ullrich, K.; Hoffmann, G. F.; Burgard, P.; Schmidt, H.; *et al*. A European Multicenter Study of Phenylalanine Hydroxylase Deficiency: Classification of 105 Mutations and a General System for Genotype-Based Prediction of Metabolic Phenotype. *Am. J. Hum. Genet.* **1998**, *63*, 71–79.

23. Janssens, S. D.; Pobedinskas, P.; Vacik, J.; Petráková, V.; Ruttens, B.; D'Haen, J.; Nesládek, M.; Haenen, K.; Wagner, P. Separation of the Intra- and Intergranular Magnetotransport Properties in Nanocrystalline Diamond Films on the Metallic Side of the Metal-Insulator Transition. *New J. Phys.* **2011**, *8*, 083008.

24. Christiaens, P.; Vermeeren, V.; Wenmackers, S.; Daenen, M.; Haenen, K.; Nesládek, M.; vandeVen, M.; Ameloot, M.; Michiels, L.; Wagner., P. EDC-Mediated DNA Attachment to Nanocrystalline CVD Diamond Films. *Biosens. Bioelectron.* **2006**, *22*, 170–177.

25. De Volder, M. F. L.; Vansweevelt, R.; Wagner, P.; Reynaerts, D.; Van Hoof, C.; John Hart, A. Hierarchical Carbon Nanowire Microarchitectures Made by Plasma-Assisted Pyrolysis of Photoresist. *ACS Nano* **2011**, *5*, 6593–6600.

26. Vermeeren, V.; Wenmackers, S.; Daenen, M.; Haenen, K.; Williams, O. A.; Ameloot, M.; vandeVen, M.; Wagner, P.; Michiels, L. Topographical and Functional Characterisation of the ssDNA Probe Layer Generated through EDC Mediated Covalent Attachment to Nanocrystalline Diamond Using Fluorescence Microscopy. *Langmuir* **2008**, *24*, 9125–9134.

27. van Grinsven, B.; Vandenryt, T.; Duchateau, S.; Gaulke, A.; Grieten, L.; Thoelen, R.; Ingebrandt, S.; De Ceuninck, W.; Wagner, P. Customized Impedance Spectroscopy Unit for Label Free Affinity Biosensors. *Phys. Status Solidi A* **2010**, *207*, 919–923.

28. Lenz, M.; Striedl, G.; Fröhler, U. Thermal Resistance, Theory and Practice; Special Subject Book January 2000: SMD Packages. Released by Infineon Technologies AG, Munich, Germany.

29. Kodama, T.; Jain, A.; Goodson, K. E. Heat Conduction through a DNA—Gold Composite. *Nano Lett.* **2009**, *9*, 2005–2009.

30. Privalov, P. L.; Ptitsyn, O. B.; Birshtein, T. M. Determination of Stability of the DNA Double Helix in an Aqueous Medium. *Biopolymers* **1969**, *8*, 559–571.

31. Gruenwedel, D. W. Salt Effects on the Denaturation of DNA - III. A Calorimetric Investigation of the Transition Enthalpy of Calf Thymus DNA in Na_2SO_4 Solutions of Varying Ionic Strength. *Biochim. Biophys. Acta* **1974**, *340*, 16–30.

32. Smirnov, I.; Shafer, R. H. Effect of Loop Sequence and Size on DNA Aptamer Stability. *Biochemistry* **2002**, *39*, 1462–1468.

33. Lettau, K.; Warsinke, A.; Katterle, M.; Danielsson, B.; Scheller, F. W. A Bifunctional Molecularly Imprinted Polymer (MIP): Analysis of Binding and Catalysis by a Thermistor. *Angew. Chem., Int. Ed.* **2006**, *45*, 6986–6990.

34. Ambia-Garrido, J.; Vainrub, A.; Pettitt, B. M. A Model for Structure and Thermodynamics of ssDNA and dsDNA near a Surface: A Coarse Grained Approach. *Comput. Phys. Commun.* **2010**, *181*, 2001–2007.

35. Wenmackers, S.; Vermeeren, V.; vandeVen, M.; Ameloot, M.; Bijnens, N.; Haenen, K.; Michiels, L.; Wagner, P. Diamond-Based DNA Sensors: Surface Functionalization and Read-Out Strategies. *Phys. Status Solidi A* **2009**, *206*, 391–408.

36. Rezek, B.; Shin, D.; Nebel, C. E. Properties of Hybridized DNA Arrays on Single-Crystalline Undoped and Boron-Doped (100) Diamonds Studied by Atomic Force Microscopy in Electrolytes. *Langmuir* **2007**, *23*, 7626–7633.

37. Wenmackers, S.; Pop, S. D.; Roodenko, K.; Vermeeren, V.; Williams, O. A.; Daenen, M.; Douheret, O.; D́Haen, J.; Hardy, A.; Van Bael, K.; *et al.* Structural and Optical Properties of DNA Layers Covalently Attached to Diamond Surfaces. *Langmuir* **2008**, *24*, 7269–7277.

38. Yang, W. S.; Auciello, O.; Butler, J. E.; Cai, W.; Carlisle, J. A.; Gerbi, J.; Gruen, D. M.; Knickerbocker, T.; Lasseter, T. L.; Russel, J. N.; *et al.* DNA-Modified Nanocrystalline Diamond Thin-Films as Stable, Biologically Active Substrates. *Nat. Mater.* **2002**, *1*, 253–257.

39. Livache, T.; Maillart, E.; Lassalle, N.; Mailley, P.; Corso, B.; Guedon, P.; Roget, A.; Levy, Y. Polypyrrole Based DNA Hybridization Assays: Study of Label Free Detection Processes *versus* Fluorescence on Microchips. *J. Pharm. Biomed. Anal.* **2003**, *32*, 687–696.

40. Melli, M.; Scoles, G.; Lazzarino, M. Fast Detection of Biomolecules in Diffusion-Limited Regime Using Micromechanical Pillars. *ACS Nano* **2011**, *5*, 7928–7935.

41. Bonnauron, M.; Saada, S.; Mer, C.; Gesset, C.; Williams, O. A.; Rousseau, L.; Scorsone, E.; Mailley, P.; Nesladek, M.; Arbault, J. C.; *et al.* Transparent Diamond-on-Glass Micro-Electrode Arrays for *Ex-Vivo* Neuronal Study. *Phys. Status Solidi A* **2008**, *205*, 2126–2129.

42. Yang, N.; Uetsuka, H.; Osawa, E.; Nebel, C. E. Vertically Aligned Diamond Nanowires for DNA Sensing. *Angew. Chem., Int. Ed.* **2008**, *47*, 5183–5185.

43. Demers, L. M.; Ginger, D. S.; Park, S. J.; Li, Z.; Chung, S. W.; Mirkin, C. A. Direct Patterning of Modified Oligonucleotides on Metals and Insulators by Dip-Pen Nanolithography. *Science* **2002**, *296*, 1836–1838.

44. Liu, H. X.; Sun, W. Q.; Chen, Q.; Xu, S. Y. Thin-Film Thermocouple Array for Time-Resolved Local Temperature Mapping. *IEEE Electron Device Lett.* **2011**, *32*, 1606–1608.

45. Wang, X. Y.; Ruther, R. E.; Streifer, J. A.; Hamers, R. J. UV-Induced Grafting of Alkenes to Silicon Surfaces: Photoemission *versus* Excitons. *J. Am. Chem. Soc.* **2010**, *132*, 4048–4049.